

STEM electron tomography in the Scanning Electron Microscope

This content has been downloaded from IOPscience. Please scroll down to see the full text.

2015 J. Phys.: Conf. Ser. 644 012012

(<http://iopscience.iop.org/1742-6596/644/1/012012>)

View [the table of contents for this issue](#), or go to the [journal homepage](#) for more

Download details:

IP Address: 192.167.170.50

This content was downloaded on 20/10/2015 at 13:09

Please note that [terms and conditions apply](#).

STEM electron tomography in the Scanning Electron Microscope

M Ferroni^{1,3}, A Signoroni¹, A Sanzogni¹, G Sberveglieri^{1,3}, A Migliori²,
L Ortolani², M Christian^{2,4}, L Masini², V Morandi²

¹ Department of Information Engineering, Brescia University,
Via Valotti 9, 25123 Brescia, Italy

² CNR-IMM Section of Bologna, via Gobetti 101, 40129 Bologna, Italy

³ CNR-INO, Via Valotti 9, 25123 Brescia, Italy

⁴ CNR-ISOF, via Gobetti 101, 40129 Bologna, Italy

Corresponding author's email: matteo.ferroni@unibs.it

Abstract. The scanning-transmission imaging mode in the SEM allows for the three-dimensional tomographic reconstruction of a specimen, starting from a set of projection images. Compressed sensing was used to solve the undetermined problem of structure reconstruction and was proven capable of overcoming the limitations arising from the sampling scheme. Reconstructions of cobalt particles within a carbon nanotube and collagen fibrils in a dermal tissue are presented, demonstrating the potential of this technique in the set of 3-D electron microscopy methods for both physical and biological science.

1. Implementation of tomography in the SEM

In conventional three-dimensional imaging methods operated in the scanning electron microscope, the volume reconstruction of a sample is retrieved from a cumulative series of images of the specimen, which is sectioned stepwise by a microtome blade or a focused beam of Ga ions during the imaging sequence [1]. This *slice-and-view* approach is capable of achieving nanometric resolution in the reconstruction of volumes as large as several cubic micrometres; however there are intrinsic limitations related to dealing with porous structures, measuring an adequate image contrast for the sample details, and maintaining a planar thin sectioning throughout the slicing process.

Recently, implementation of the scanning-transmission (STEM) imaging mode in the SEM has allowed the investigation of the inner structure of thin samples at low beam energy [2-4], and established the possibility of reconstructing the spatial mass distribution, similar to the approach to electron tomography (ET) in the TEM [5]. Because this method requires a projection scheme, reconstruction of the specimen relies on the backprojection algorithm of tomography [6] and could take advantage of the theory of compressed sensing to reduce the artifacts produced by the inevitably limited and incomplete series of experimental projections [7].

In this paper, we present the experimental approach and application of this tomographic method implemented in the SEM.



2. Experimental set-up and reconstruction workflow

ET in the SEM requires that the specimen is suspended to allow transmission of the electrons, while rotating under the electron beam to produce the series of projection-images. A dedicated segmented detector, capable of *Bright/Dark Field* imaging, and a specimen holder have been set up for the purpose, an arrangement that benefits from the absence of post-specimen imaging lenses in the SEM chamber. Owing to the strong influence of the mass-thickness of the sample on the beam scattering angle, the assembly of the holder and electron detector is fundamental to preserve the monotonic increase of image contrast upon tilting the sample, which is required for the subsequent reconstruction.

The tomographic workflow, summarized in **Figure 1**, is based on the conventional inverse-Fourier backprojection and uses the prior knowledge about the sparsity of the object under investigation to refine the tomogram, according to the Compressed Sensing (CS) approach to signal reconstruction.

Owing to the linear orthographic nature of the projections and their alignment, the tomographic reconstruction of the volume $r(x,y,z)$ can be decomposed into a *slice-by-slice* problem from the stack of lines of the projection images. Projections are considered as samples of the 2D Fourier transform of the volume slice, and arranged to form a polar sampling (with a missing wedge in our case). From this starting point, the effective backprojection is carried out by the Non-Uniform FFT [8], which offers a useful initialization and effectively operates in a CS-based refinement.

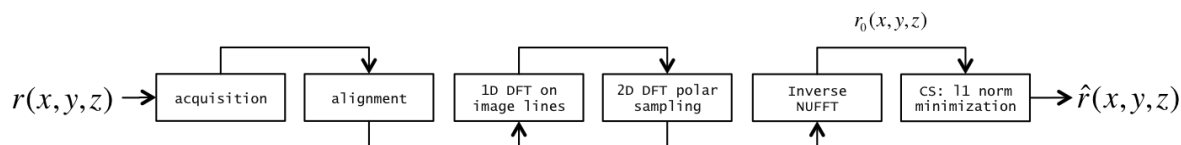


Figure 1 Schematic workflow of the reconstruction process.

According to the theory of CS applied to electron tomography, the initial tomogram $r_0(x,y,z)$ is refined by considering some degree of sparsity in both image and gradient domains [8]. Despite the presence of reconstruction artifacts caused by the limited number of experimental projections and the missing wedge, the method can converge to an accurate reconstruction $\hat{r}(x,y,z)$ and was here applied to samples with different characteristics, in order to test its feasibility in both physical and biological science. The regularization parameters have been optimized accordingly.

3. Application in materials science: carbon nanotubes and cobalt nanoparticles

Figure 2 (*Left*) shows a STEM image of a multi-walled carbon nanotube (CNT) filled with cobalt particles supported by a TEM holey carbon film grid.

A series of 53 projections was acquired by tilting the sample through -60° to $+60^\circ$ at 2° steps. The best image contrast for the visualization of the support, the CNT, and the Co particles was obtained for the *Dark-Field* imaging, where only the annular part of the detector was activated. The Region of Interest (ROI) selected for the reconstruction is marked by a red box, and the preliminary alignment of the tilt series was carried out by maximizing a rotation compensated image cross-correlation. The result of the reconstruction is presented in **Figure 2** (*Center and Right*). The lateral views clearly separate the Co particles within the light carbon structure. The reconstruction has been refined through compressive sensing with optimized regularization parameters for both the image and gradient domains [9]. In this case, the marked separation in the elemental composition and the localization of Co into particles account for the recorded predominant sparsity in the gradient domain.

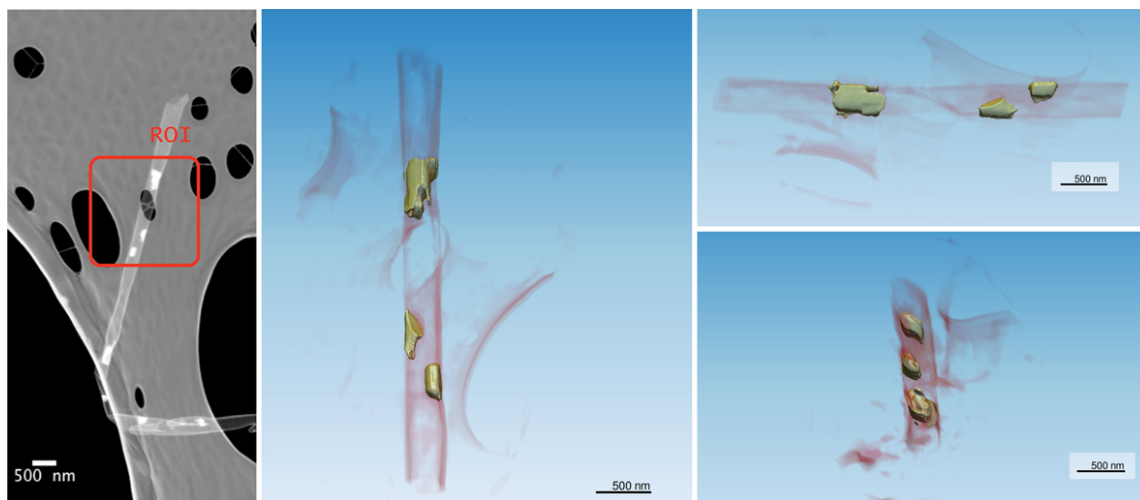


Figure 2 Tomographic reconstruction of a materials science sample. (*Left*) STEM image from the tilt series of a CNT filled with Co particles (*Center*) Front-view of the reconstructed tomogram (*Right*) Two side views of the tomogram showing the cobalt particles inside the CNT.

4. Application in biology: dermal tissue

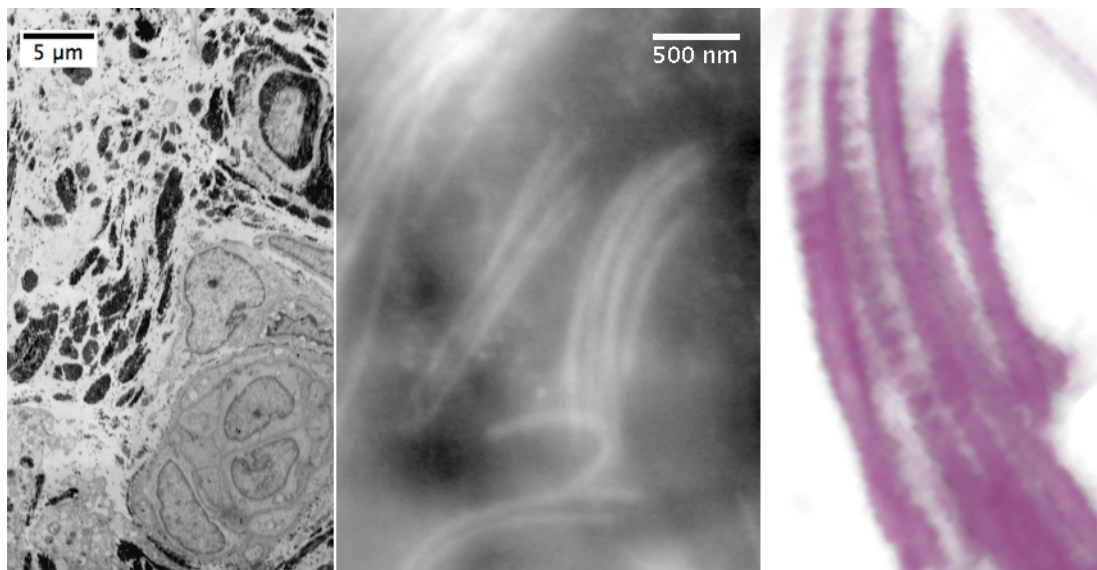


Figure 3 STEM images and reconstruction of a biological sample: (*Left*) Panoramic view of cellular structures and collagen fibers in human derma (*Center*) Image from the tilt series of the collagen bundle selected for tomographic reconstruction (*Right*) Detail from the CS-refined tomogram of the collagen bundle, showing the characteristic periodical (approx. 64 nm) striation along the fibrils.

Figure 3 highlights the structure of the dermal tissue as revealed by the STEM imaging mode in the SEM. The panoramic *Bright-Field* image of a 700 nm-thick specimen shows cellular membranes together with bundles of collagen fibrils. By operating the STEM in the *Dark-Field* mode with a 20 kV beam, the contrast for the fibrils is significant and adequate for the tomographic workflow.

In this sample, the region selected for the reconstruction encloses a small bundle of collagen fibrils. Starting from 91 projections covering the angular range between -50° and $+40^\circ$, at $40000\times$ magnification, the CS-refinement of the tomogram revealed the known transverse striation of the fibrils, which is visible as a periodical contrast modulation in the visualized tomogram. The resulting resolution was consistent with Crowther's estimation of 24 nm, which ideally requires the projections to be noise-free, perfectly aligned, and covering the entire angular range.

Owing to the complex characteristics of the biological system under investigation, optimization of the CS regularization parameters occurred for a dominant influence attributed to the sparsity term in the image domain.

5. Concluding remarks

The proposed approach exploits the flexibility of the SEM platform and showcases the potential of SEM tomography for the 3D analysis of volumes. This low-energy implementation of electron tomography, based on STEM imaging, is capable of reconstructing small samples and dealing with specimens featuring uneven thickness, or large contrast variations. The flexibility of optimization through compressed sensing allows the analysis of a large variety of samples.

The limit in resolution is determined by the probe size of the microscope, the specimen composition and thickness, and the number of projections that can be acquired without significant beam damage of the sample. The proposed system can be applied for both biological and physical science and performs at smaller volume and higher resolution ranges compared to conventional techniques.

References

- [1] Cantoni M and Holzer L 2014 *MRS Bull* **39** 354–60
- [2] Merli P, Morandi V and Corticelli F 2003 *Ultramicroscopy* **94** 89–98
- [3] Morandi V, Merli P and Ferroni M 2006 *J Appl Phys* **99** 043512
- [4] Morandi V, Merli P G and Quaglino D 2007 *Appl Phys Lett* **90** 163113
- [5] Bals S, Van Aert S and Van Tendeloo G 2013 *Current Opinion in Solid State & Materials Science* **17** 107–14
- [6] Kak A C and Slaney M 1999 *Principles of Computerized Tomography* (New York: IEEE press) pp 1–26
- [7] Leary R, Saghi Z, Midgley P A and Holland D J 2013 *Ultramicroscopy* **131** 70–91
- [8] Fessler J A and Sutton B P 2003 *Signal Processing, IEEE Transactions on Signal Processing* **51** 560–74
- [9] Thomas J M, Leary R, Midgley P A and Holland D J 2013 *J Colloid and Interface Science* **392** 7–14